TOPOLOGY OPTIMIZATION STUDY ON FLOW AND HEAT TRANSFER PERFORMANCE OF TURBINE PIN-FIN COOLING STRUCTURE

Xiao WANG, Pingting CHEN*, JunKui MAO

College of Energy and Power Engineering, Nanjing University of Aeronautics and Astronautics.
No.29, Yudao Street, Nanjing, Jiangsu, 210000, P.R. China

* Corresponding author; E-mail: cpt09@nuaa.edu.cn

Pin-fin cooling is commonly used in the trailing edge area of gas turbines to enhance heat transfer and improve the structural strength of the blades. At present, researchers mainly use size or shape optimization to improve the flow heat transfer performance of traditional cylindrical pin-fin cooling. However, the optimization potential of pin-fin cooling can be more fully exploited through topology optimization methods. On the basis of the cylindrical pin-fin structure, the topology optimization method based on level set is used to improve the heat transfer and pressure loss performance of the cooling channel of the column pin-fin, and the research results show that the shape of the optimized channel spoiler element presents a tadpole-shaped structure downstream of the column pin-fin. These tadpole-shaped structures modify the flow, leading to acceleration along the flow direction and a reduction in the low-velocity wake region. Consequently, the Nusselt number (Nu) gradually increases along the flow direction. The optimized model achieves the highest heat transfer intensity with a relatively low pressure loss, resulting in the best overall thermo-hydraulic performance.

Key words*: gas turbine, turbine blade, topology optimization, pin-fin, level set method, heat transfer and pressure loss*

1. Introduction

The narrow space within the trailing edge region of internal turbine channels makes cooling in this area particularly challenging. To ensure the structural strength and fulfill the cooling demands, the pin-fin cooling design that connects the suction and pressure surfaces in the trailing edge region is often employed **Error! Reference source not found.**. Researches on the effects of pin-fin cooling structures mainly focus on the effect of geometric factors such as the height-to-diameter ratio, spacing-to-diameter ratio, arrangement methods, and pin-fin shapes on the aero-thermal performance of the pin-fin cooling structures, as well as their optimization using the parametric optimization algorithms **Error! Reference source not found.Error! Reference source not found.**.

A lot of researchers conducted parametric optimization for pin-fin geometry designs [4-8]. Metzger et al.**Error! Reference source not found.** found that staggered arrangements result in higher heat transfer coefficients compared to aligned arrangements. Pandit et al. **Error! Reference source not found.** demonstrated the diamond pin-fin exhibits the best enhancement in heat transfer compared to circular, triangular, and hexagonal pin-fin. Yalçınkaya et al. **Error! Reference source not found.** found that elliptical pin-fins, when used in conjunction with extended jets, can not only effectively enhance heat transfer efficiency but also achieve efficient cooling performance with lower pressure loss.In addition, the study by Yalçınkaya et al. **Error! Reference source not found.** indicates that using elliptical pin fins with a relatively low height in combination with a double-row arrangement can achieve maximum enhancement in heat transfer efficiency for jet impingement cooling systems, while also realizing a more uniform heat transfer distribution.However, when considering both heat transfer and pressure loss characteristics, Chyu et al.**Error! Reference source not found.** discovered that circular pin-fin arrays are more suitable for heat exchangers when balancing heat transfer and pressure loss.

Although significant progress has been made in the parametric optimization of pin-fin performance, size or shape optimization can only achieve the objective function by adjusting points or boundaries of the structure, which does not allow for changes in geometry topology and limits the potential for further optimization of pin-fin cooling performance. Meanwhile, the rapid maturation of additive manufacturing technology has made it possible to create cooling structures with complex and irregular geometries **Error! Reference source not found.**. For aircraft engines and other large, complex structural components, such as engine turbine blades, introducing additive manufacturing into the field of turbine blade casting can significantly reduce structural complexity, enabling mold-free fabrication of cores and shells, and providing a new approach for the rapid manufacturing of hollow turbine blades **Error! Reference source not found.**. Laser and electron beam selective melting technologies can be applied to the manufacturing of components such as aircraft guards, fuel nozzles, and turbine blades; moreover, additive manufacturing techniques can be used for repairing and validating critical structures such as titanium alloy frames and integrated bladed disks (blisks) **Error! Reference source not found.**. The research team led by Professor Di Chen Li **Error! Reference source not found.** at Xi’an Jiaotong University has achieved significant breakthroughs in areas including core-shell integrated rapid forming of turbine blades, ceramic mold preparation, high-temperature mechanical property control of molds, and full-process precision control of blade dimensions. They have established a rapid preparation system for core-shell integrated molds for hollow turbine blades based on stereolithography (SLA) 3D printing.Thus, topology optimization **Error! Reference source not found.** has gained increased attention, with the development of additive manufacturing technology, enabling a more thorough exploration of the design space for pin-finned cooling channels.

Topology optimization is a method that uses material distribution as a design variable to find the optimal material distribution, corresponding to the objective function within a design domain, based on given boundary conditions and constraints. Initially, topology optimization was commonly used in the field of structural mechanics **Error! Reference source not found.**. In recent years, with advancements in computer technology, topology optimization has also found applications in fluid dynamics **Error! Reference source not found.**. Early studies on fluid-based topology optimization primarily focused on laminar flow or simplified turbulence using the Darcy formula **Error! Reference source not found.**. Borrvall and Petersson **Error! Reference source not found.** conducted pioneering research in the field of fluid topology optimization, achieving topology structures for Stokes flow. In terms of topology optimization considering turbulence, Research by An Li **Error! Reference source not found.** indicated that using a simplified turbulent model like the Darcy formula for topology optimization significantly improved the flow channel structure in reducing average temperature and flow loss performance. Yoon et al. [17-18] proposed a finite element topology optimization method based on the Spalart-Allmaras and k-ε turbulence models, showing that the optimization model considering turbulence effects outperformed the model using the frozen turbulence assumption. Thus, topology optimization based on turbulence models is increasingly becoming a key development direction in engineering applications, as computational fluid dynamics simulation ability increases.

In terms of topology optimization methods, the widely used approaches in fluid dynamics are the variable density method and the level set method. Regarding the application of the variable density method, research by Yeranee et al. [19-20] has shown that density-based topology optimization can be used to optimize pin-fin cooling structures. Wang et al. **Error! Reference source not found.** applied a density-based method for the topological optimization of battery cold plates. The results show that the optimized cold plate can effectively reduce flow resistance and fluid energy loss, thereby decreasing the energy consumption required for pumping the coolant and significantly improving energy efficiency.Pandey et al. **Error! Reference source not found.** performed topology optimization on the heat sink using a density-based method. The optimized structure exhibits more efficient heat transfer capability under high flow rate conditions, while effectively reducing temperature stratification and improving thermal uniformity in the system.As for the application of the level set method, Duan et al. **Error! Reference source not found.** applied the variational level set method to fluid topology optimization, producing results similar to those obtained with previous density-based methods. Jiang Zirun **Error! Reference source not found.** pointed out that density-based topology optimization methods struggle to accurately describe the boundaries between fluid and solid materials, whereas the boundaries obtained through level set optimization are clear and smooth, making it a better choice for fluid topology optimization. Therefore, applying the level set method to the topology optimization of pin-fin cooling structures is expected to further improve the flow and heat transfer characteristics of pin-finned channels.

In terms of setting optimization objectives, Haertel et al. **Error! Reference source not found.** optimized the design of heat exchangers by minimizing pressure loss within the channels. Their research indicated that the heat transfer enhancement from the pressure loss minimization model is due to the streamlined shape of the optimized structure (similar to shapes like teardrop or oval), which guides the fluid to flow slightly inclined within the channel, thereby increasing the contact area between the fluid and the solid, enhancing heat transfer. Therefore, adopting pressure loss minimization as the optimization objective is expected to be a viable solution.

In summary, the topology optimization of pin-fin cooling needs to consider both heat transfer performance and pressure loss performance, while topology optimization methods can better exploit the design space of pin-finned channels.The level set-based topology optimization methods have shown advantages in fluid dynamics topology optimization due to their ability to accurately describe the boundaries between fluid and solid materials. However, existing literature has not yet applied the level set method to the topology optimization of turbine cooling. Therefore, to fully leverage the advantages of the level set method, the current study employs a level set-based topology optimization approach to improve the heat transfer performance and pressure loss performance of pin-finned cooling channels. The fluid dynamics solver uses the k-ε turbulence model. With pressure loss minimization as the objective function, the pin-finned cooling channel under a Reynolds number of Re=10000 is optimized to achieve a improvement in both heat transfer and pressure loss performance.

2. Pin-finned cooling channel model

Figure 1(a) shows the computational domain of the pin-finned cooling channels used in this study, using the baseline cylindrical pin-fin case as an example. Figure 1(b) depicts the four regular pin-fin design, including the baseline cylindrical pin-fin, the large diameter cylindrical pin-fin, the diamond pin-fin, and the triangular pin-fin. The latter three structures (large diameter cylindrical, diamond, and triangular) are designed to have the same solid volume fraction as the model resulting from the subsequent topology optimization of the baseline cylindrical pin-fin, allowing for a fair comparison.

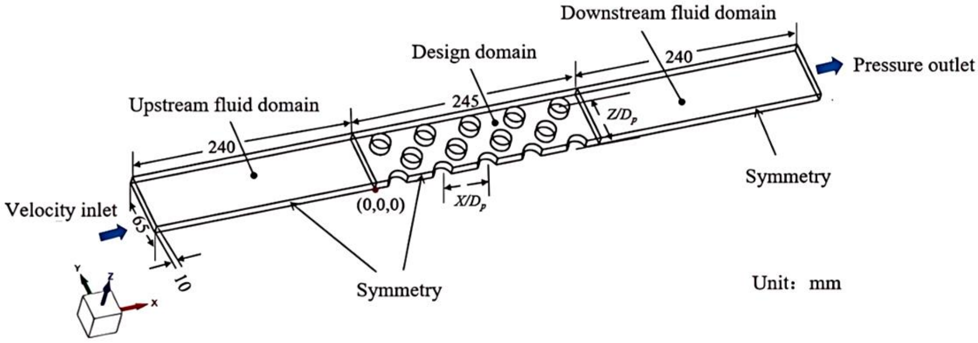

(a) The computational domain of the pin-finned cooling channels

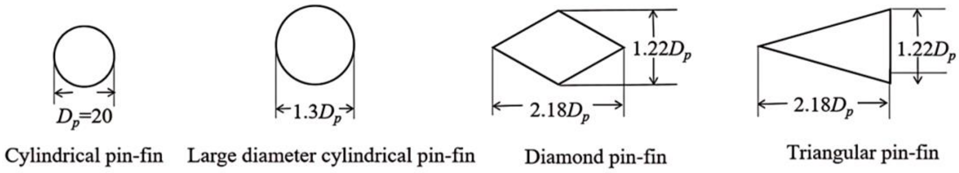

(b) The four regular pin-fin's shape and size

Fig. 1 Geometry Model: (a) Computational domain of the pin-finned cooling channels (baseline cylindrical case shown). (b) Geometries and dimensions of the four regular pin-fin designs investigated

The channel is divided into the following regions: (1) Upstream fluid domain, (2) Design domain, (3) Downstream fluid domain. The lengths of the upstream and downstream domains are 240mm, while the design domain's length is 245mm. The origin coordinate is marked in Figure 1, located at the lower left corner of the design domain. A velocity boundary condition is applied at the inlet, and the inlet velocity is evaluated based on the experimental Reynolds number, which is defined as follows: $Re=\rho U_{in}D_h/\mu$. A static pressure is specified at the outlet boundary. The upper and lower walls of the design domain, as well as the surface of the pin-fins are set as no-slip isothermal wall conditions **Error! Reference source not found.** (temperature at 313 K). Symmetry boundary conditions are employed to reduce overall computational costs, while the remaining boundaries are set as adiabatic no-slip wall boundary conditions. Detailed geometric and boundary condition parameters are shown in Table 1.

Tab. 1: Model Parameters

Parameters	value
Height-to-diameter Ratio(H/D_p [-])	0.5

Spanwise Spacing-to-diameter Ratio(Z/D_p [-])	2.5
Streamwise Spacing-to-diameter Ratio(X/D_p [-])	2.5
Reynolds Number(Re [-])	10000
Fluid Density(ρ [kg/m3])	1.204
Fluid Dynamic Viscosity(μ [Pa·s])	1.83×10^{-5}
Hydraulic Diameter(D_h [mm])	18.5

3. Level set-based topology optimization method

3.1. Level set method

The current optimization process uses the improved level set equations, as follows:

$$\frac{\partial\varphi}{\partial\tau}+F\left|\nabla\varphi\right|=S \tag{1}$$

$$F=\frac{\bar{v}V}{\sum_k\left|\bar{A}_k\right|} \tag{2}$$

$$S=-\omega\ (1-\mathrm{sign}(\bar{v})\varphi)\bar{v} \tag{3}$$

where φ is the level-set variable with values ranging between -1 and 1 (φ = 0, it represents the fluid-solid boundary; φ > 0, it represents the region occupied by the fluid material; φ < 0, it represents the region occupied by the solid material), and ω is the constant source strength. . If ω = 0, new solid material can only form on existing domain boundaries or initial solid regions. If ω > 0, solid material can nucleate anywhere within the optimization domain.

The augmented Lagrangian method is employed to transform the constrained optimization problem into an unconstrained optimization problem. The augmented Lagrangian function is defined as follows:

$$L(x,\lambda)=f(x)+\sum_i\varphi(c_i,\lambda_i^k,\beta) \tag{4}$$

$$\varphi(c,\lambda,\beta)=\begin{cases}\lambda c+\dfrac{\beta}{2}c^2 & c>0\\ 0 & c\le 0\end{cases} \tag{5}$$

After each iteration, the Lagrange multipliers are updated as follows:

$$\lambda_i^{k+1}=\begin{cases}\lambda_i^k+\beta c_i & c_i>0\\ 0 & c_i\le 0\end{cases} \tag{6}$$

The material distribution is defined using the hyperbolic tangent function of the level set variable:

$$\chi=0.5\times(1+\tanh(\frac{\varphi}{\delta}))$$
$$\chi=\begin{cases}1 & x\in\Omega_{fluid}\\ 0 & x\in\Omega_{solid}\end{cases} \tag{7}$$

where χ is a binary function constructed from the level set function, used to indicate whether a given point x in the computational domain belongs to a specific material. This function effectively distinguishes between different material regions on either side of an interface. When $\chi=1$, the point is considered to be within the material of interest, and corresponding calculations can be carried out based on the actual physical properties of that material. In contrast, when $\chi=0$, the point is regarded as either void or composed of a non-target material, which helps account for effects such as porosity or material heterogeneity in numerical simulations. This representation not only preserves the smoothness of the interface description but also facilitates efficient computation in finite element analysis or other numerical methods.

Using Brinkman penalization to model the blockage by the solid regions, this penalization treats the solid as a porous medium with very low porosity:

$$\frac{\partial \rho v}{\partial t} + \nabla \cdot (\rho v \otimes v) = -\nabla \cdot \sigma - \alpha(1-\chi) \tag{8}$$

where δ is used to control the thickness of the interface, with a value of 0.1, and α is the Brinkman penalty magnitude, which must be sufficiently large to reduce the velocity within the solid to an acceptable tolerance, hence it is set to 1e7.

3.2. Mathematical optimization model

This study selects the minimization of pressure loss as the optimization objective to improve the overall heat transfer performance of the cooling channel [19-20]**Error! Reference source not found.**. The expression for pressure loss is as follows:

$$\Delta p = p_{in} - p_{out} \tag{9}$$

This study does not impose temperature constraints or volume constraints. The mathematical optimization model is as follows:

$$\begin{aligned} &Minimize\text{:}\ \ \Delta p(\chi, S_1(\chi)) \\ &Subject\ to \quad R(\chi, S_1(\chi)) = 0 \\ &0 \le \chi(x) \le 1, \forall x \in \Omega_{in} \end{aligned} \tag{10}$$

The topology optimization and CFD calculations in this paper were conducted using the commercial software Simcenter STAR-CCM+.

4. Validation of flow and heat transfer simulation methods

The flow and heat transfer simulation methods are validated by comparing the simulated *Nu* and friction coefficient (*f*) against the measured data by Rao et al. **Error! Reference source not found.** for a channel with pin-fins. The *Re* range for this simulation validation is *Re* = 10000 ~ 20000.

The averaged *Nu* is used to validate the heat transfer performance, and definition is as follows:

$$Nu = \frac{hD_h}{k_f} \tag{11}$$

$$h = \frac{q}{T_w - T_c} \tag{12}$$

where k is the thermal conductivity of the fluid, h is the heat transfer coefficient, q is the wall heat flux, T_w is the wall temperature, and T_c is the bulk fluid temperature.

Figure 2 shows the averaged *Nu* measured by Rao et al. **Error! Reference source not found.** and simulated in the current study with different *Re* values. For the pin-fins channel, the *Nu* increases with the increase of *Re*. At the *Re* of 10,000, the maximum error between the numerical and experimental data is approximately 6.9%, which is acceptable for the current study.

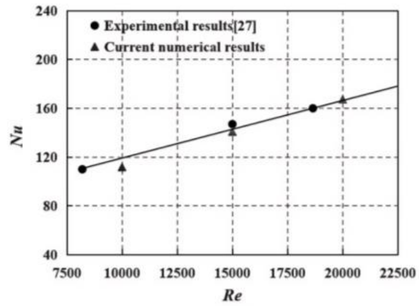

Fig. 2 Comparison of Rao et al. [27] experimental results with the current numerical results on the averaged *Nu*

The friction coefficient is used to compare the pressure loss between the experimental data and the numerical data, which is defined as follows:

$$f = \frac{2D_h}{\rho {U_{in}}^2}\left|\frac{\Delta p}{dx}\right| \tag{13}$$

Figure 3 shows the comparison between the friction factor values measured by Rao et al. [27]. and that simulated in the current study. As the *Re* increases, the friction coefficient gradually decreases. Throughout range of *Re* studied here, the friction coefficient obtained in this study is higher than the experimental data, with a maximum error of approximately 7.7%. The rate of decrease in the friction coefficient simulated in this study is similar to that of the experimental data, therefore, the friction coefficient obtained from this numerical model is acceptable for the optimization in this research.

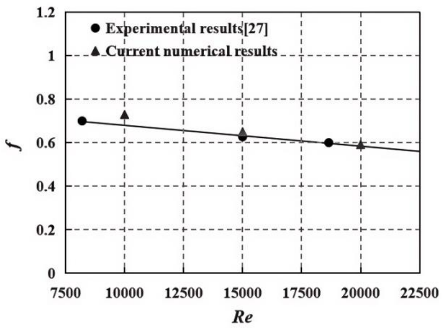

Fig. 3 Comparison of Rao et al. [27] experimental results with the current numerical results on the friction factors (*f*)

5. Results and discussion

5.1. Iterative History

Figure 4 shows the trend of the pressure loss and the solid volume fraction changes throughout the optimization iterative process. In the initial stage, the pressure loss increases with the solid volume

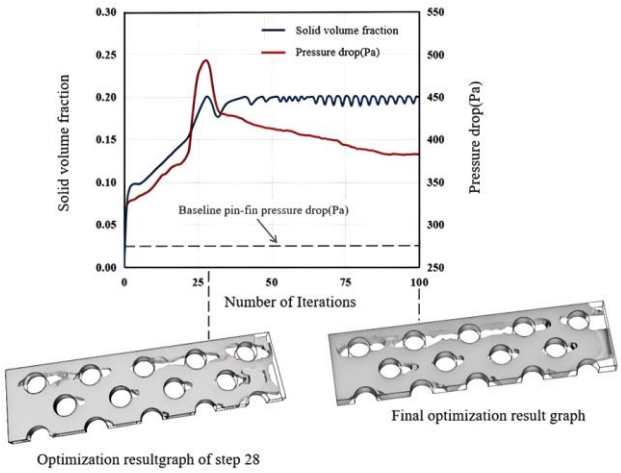

Fig. 4 Iteration history of solid volume fraction and pressure drop during the topology optimization process. Inset images show the geometry at iteration 28 and the final converged design

fraction increases. This phenomenon peaks at iteration step 28, where both the solid volume fraction reaches its maximum and the pressure loss correspondingly rises to its highest value. The optimization results at step 28 provide a crucial starting point for subsequent iterations, marking the transition to more refined pressure loss control. Subsequently, while keeping the solid volume fraction essentially constant, the pressure loss gradually decreases until it ultimately stabilizes and converges. The final converged pressure loss value is approximately 28.7% lower than that at step 28.

5.2. Optimized channel geometry

The channel geometry obtained from topological optimization is shown in Figure 5. It can be observed that the shape of the optimized channel disturbance elements varies in the streamwise direction, lateral direction, and the height of the pin-fin direction, according to varied local flow and heat transfer characteristics. The optimized pin-fin elements generate tadpole shapes with varying sizes and configurations in each row. In the first row, tadpole shapes form at the top and bottom of the pin-fins. In the second and third rows, the tadpole shapes at the top of the pin-fins disappear, while those at the bottom still remain. In the fourth row, tadpole shapes form again at both the top and bottom of the pin-fins, and the shapes of the pin-fins remain almost the same until the eighth row. Large solid structures are optimized at the channel's downstream part, meanwhile, the pin-fin structures near the channel wall merge. The solid volume ratio of the optimized channel is 0.36, with an increase of 0.14 compared to the baseline cylindrical pin-fin.

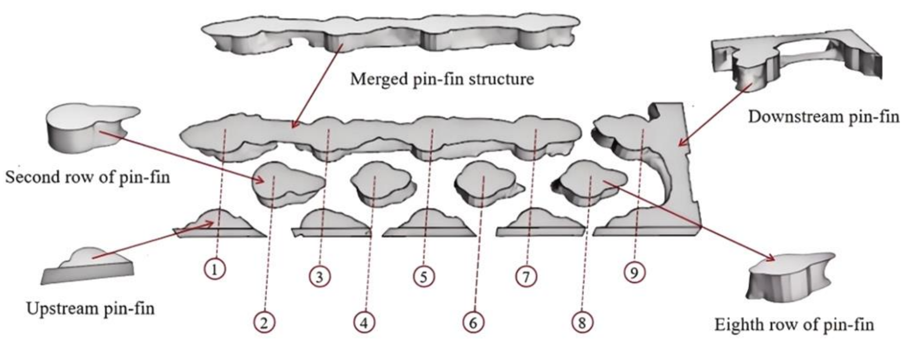

Fig. 5 The optimized channel geometry

The optimized channel structure has an irregular geometry, but the porous features are not yet apparent. Therefore, processes such as casting and additive manufacturing are more feasible.

5.3. Flow characteristics

The solid volume fraction of the optimized channel increases compared to that with the baseline cylindrical pin-fin elements. Thus, the channels with matched solid volume fraction of the optimized model, using the cylindrical pin-fin with large diameter, the diamond pin-fin, and the triangular pin-fin are added to the current study to compare the aero-thermal performance with the optimized design, as shown in Figure 1.

Figure 6 shows the velocity distributions of the five studied pin-fin geometries at z = 10 mm (the mid-section of the channel). It can be observed that the velocity gradually increases from the inlet to the outlet, as the pin-fin elements cause disturbances in the fluid flow. Due to the influence of the wake, low-velocity regions appear behind each pin-fin element.

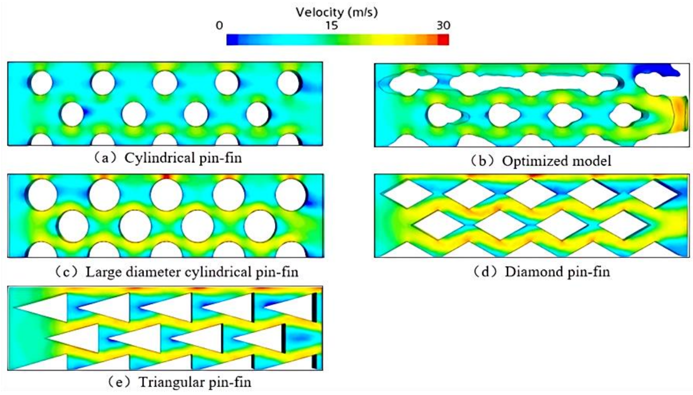

Fig. 6 Velocity distributions at z=10mm for the for the channels with different pin-fin designs

The pin-fin structure significantly affects the local flow velocity distributions. It can be observed that an acceleration zone forms on the lateral sides of the cylindrical pin-fin. Compared to the cylindrical pin-fin, the diamond and triangular pin-fins exhibit higher velocities on the lateral sides, which is attributed to that the shapes promote strong flow separation. In both cases for the diamond and triangular pin-fin designs, the low-velocity regions behind the pin-fins are more pronounced. The large diameter of the cylindrical pin-fins results in a large volume fraction, leading to a narrower flow channel, which increases the velocity on the lateral sides. Due to the interference of the tadpole-shaped structure with the flow, the low-velocity region in the wake of the optimized model is reduced, and higher local velocities can be observed downstream the pin-fin elements compared to the cylindrical pin-fin.

By comparison, the large diameter cylindrical pin-fins may increase pressure loss due to greater flow blockage. The diamond and triangular pin-fins promote higher turbulence, which could enhance heat transfer; however, the resistance caused by the pin-fins may lead to higher pressure losses.

The relative friction coefficient (f/f_0) is defined by dividing the f with the smooth channel friction resistance coefficient (f_0). The f_0 is defined as follows [26]:

$$f_0 = (0.79\ln \mathrm{Re} - 1.64)^{-2} \tag{14}$$

Figure 7 shows a comparison of the pressure loss for each model studied. The baseline cylindrical pin-fins exhibit the lowest pressure loss, followed by the optimized model. The high pressure losses associated with the diamond and triangular pin-fins can be attributed to the resistance caused by their shapes. The pressure loss for the baseline cylindrical pin-fins is approximately 35.1% lower than that of the optimized model, while the pressure losses for the large diameter cylindrical pin-fins, diamond pin-fins, and triangular pin-fins are approximately 53.9%, 232.7%, and 486.0% higher than that of the optimized model, respectively.

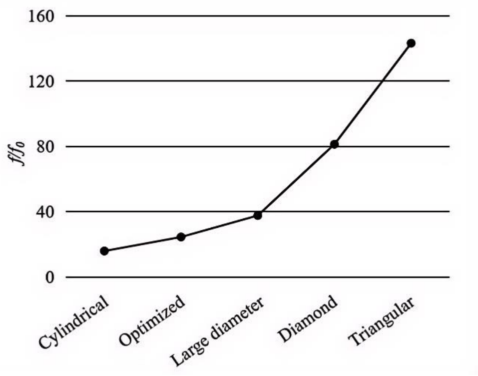

Fig. 7 Comparison of relative friction coefficients for the channels with different pin-fin designs

5.4. Heat transfer characteristics

Figure 8 shows the *Nu* distribution on the column ribbed surface and the upper and lower end walls of all models. Regions of larger *Nu* form on both sides of the pin-fins due to the acceleration of the airflow as the flow channel narrows. Regions of smaller *Nu* form behind the pin-fins because the airflow separates from the pin-fin surfaces, creating separation vortices as shown in Figure 9, which results in lower airflow velocity behind the pin-fins.

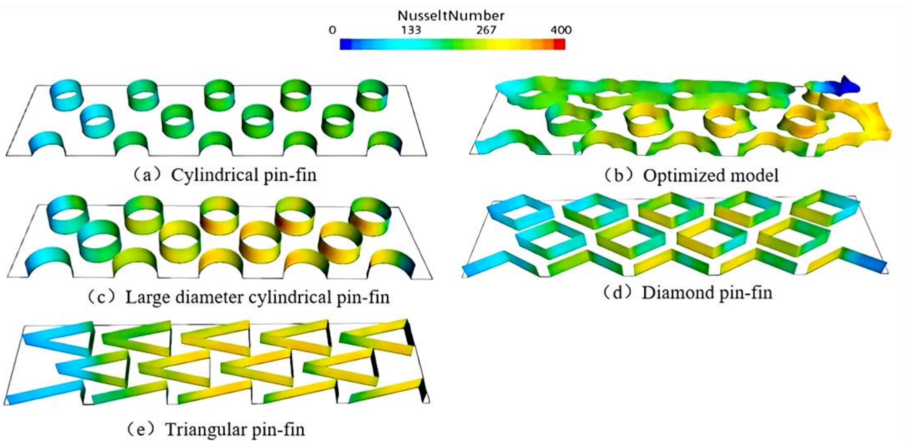

(A) *Nu* distribution diagram on the surface of column pin-fins

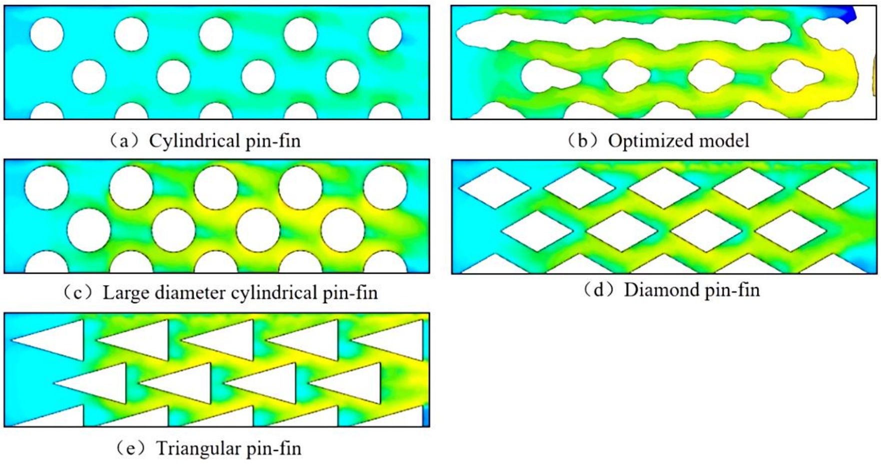

(B) *Nu* distribution diagram on the upper endwall

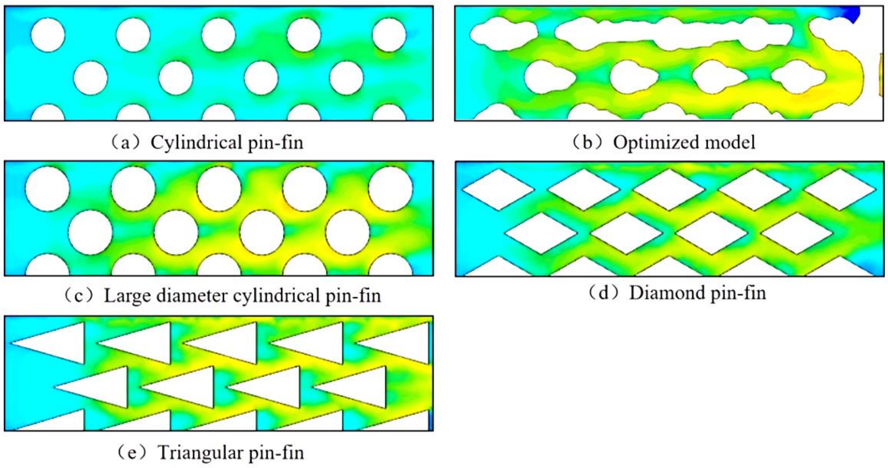

(C) *Nu* distribution diagram on the lower endwall

Fig. 8 *Nu* distribution on the pin-fins surfaces and upper/lower endwalls of various models

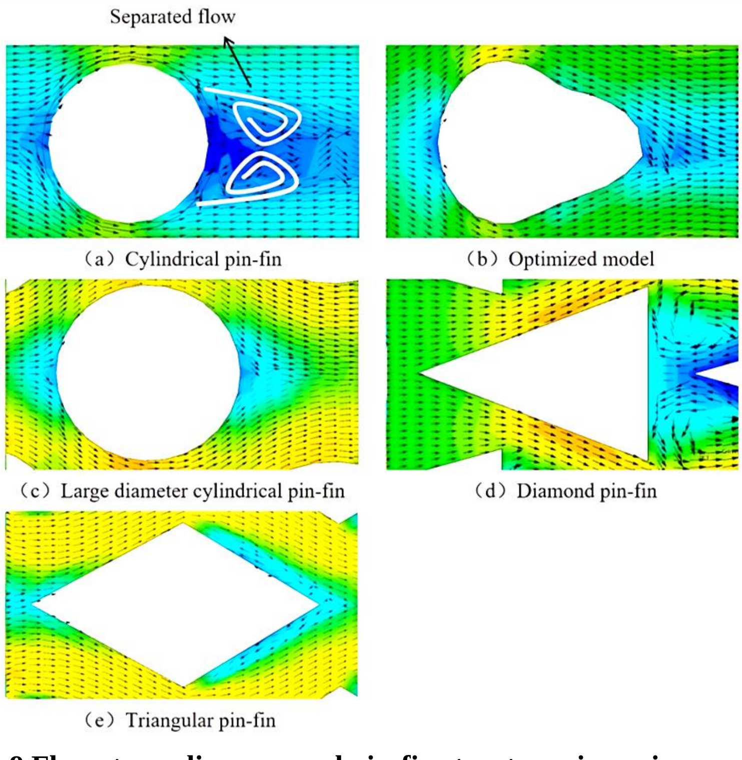

Fig. 9 Flow streamlines around pin-fin structures in various models

For cylindrical pin-fins, the *Nu* at the upstream region of the channel show a slow increasing trend. This is due to the lower turbulence level at the inlet, resulting in a minimum *Nu* at the entrance. Starting from the second row, the heat transfer coefficient gradually increases because the disturbances caused by the upstream pin-fins enhance the mixing of the airflow. Once the mixing between the airflows reaches a certain level, the enhancement of heat transfer cannot continue, which is why the *Nu* downstream does not show a further increasing trend. The diamond and triangular pin-fins exhibit a similar trend, but their *Nu* are higher than that of the baseline cylindrical pin-fins, primarily because their shapes promote stronger separated flow. The large diameter cylindrical pin-fins create a strong flow impact due to their size as the fluid flows over them, thereby increasing heat transfer, resulting in a higher *Nu* than that of the baseline cylindrical pin-fins. The pin-fins obtained through topological optimization show a trend of gradually increasing *Nu* along the streamwise direction. This is mainly because the velocity field resulting from topological optimization exhibits a continuous acceleration effect along the flow direction, along with a reduction in the low-velocity region in the wake area.

The reference Nusselt number (Nu_0) defined by the Dittus-Boelter correlation is used to normalize the *Nu*, resulting in the relative Nusselt number (Nu/Nu_0), which measures the enhancement of heat transfer by pin-fin. The Dittus-Boelter correlation **Error! Reference source not found.** is as follows:

$$Nu_0 = 0.023 Re^{0.8} Pr^{0.4} \tag{15}$$

Figure 10 shows a comparison of area averaged Nu/Nu_0 for all models. Among the different pin-fin shapes, the baseline pin-fin channel features the smallest area averaged Nu/Nu_0, while the optimized model features the highest. The area averaged Nu/Nu_0 for the large diameter pin-fin and triangular pin-fin are very close to each other. The area averaged Nu/Nu_0 for the baseline cylindrical pin-fin, the large diameter cylindrical pin-fin, the diamond pin-fin, and the triangular pin-fin are approximately 32.7%, 4.7%, 12.5%, and 4.4% lower than that of the optimized model, respectively.

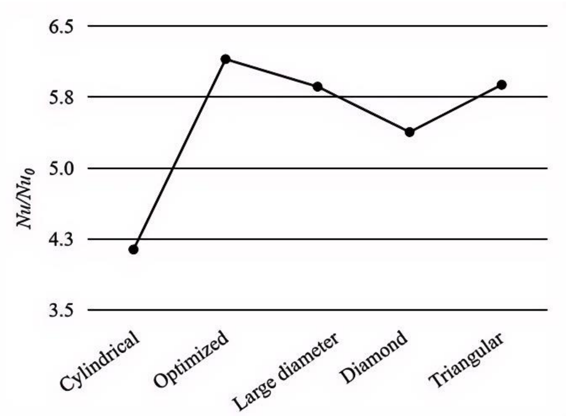

Fig. 10 Comparison of Nu/Nu_0 between the pin-fins surfaces and the upper/lower endwalls for the channels with different pin-fin designs

Considering that the heat transfer areas are inconsistent among the five models studied, the Nu_T is defined by multiplying the area averaged *Nu* with the heat transfer area values, to evaluate the heat transfer performance of the five channels. The Nu_T is expressed as follows:

$$Nu_T = Nu \times A_0 \tag{16}$$

where A_0 is the area of the upper and lower walls and the surface of the pin-fins.

Figure 11 presents the Nu_T for the five models. When compared to the results in Figure 10, a similar overall trend can be observed. The results indicate that the heat transfer intensity of the cylindrical pin-fin, large diameter cylindrical pin-fin, diamond pin-fin, and triangular pin-fin is approximately 28.8%, 7.4%, 9.5%, and 1.8% lower than that of the optimized model, respectively.

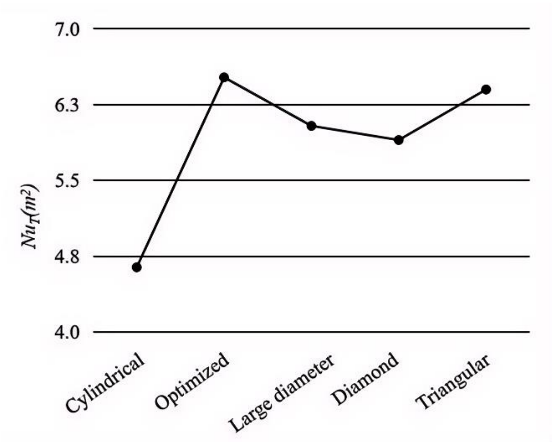

Fig. 11 Comparison of Nu_T for the channels with different pin-fin designs

5.5. Thermal performance parameter

The overall thermal performance is measured using the thermal performance parameter **Error! Reference source not found.**, which is defined as follows:

$$TF = \frac{Nu / Nu_0}{(f / f_0)^{1/3}} \tag{17}$$

Figure 12 shows the thermal performance parameters for the five studied pin-finned channels. Compared to the diamond and triangular pin-fins, the cylindrical pin-fins exhibit lower heat transfer intensity but very small pressure loss, resulting in higher overall thermal performance. The large diameter cylindrical pin-fins provide a greater cooling surface than the cylindrical pin-fins, increasing heat exchange with the surrounding fluid and thereby enhancing the thermal performance. The channel structure obtained through the level set topology optimization method alters the flow and heat transfer characteristics of the pin-fin channels, resulting in the optimized model having the highest heat transfer intensity and lower pressure loss, demonstrating the best overall thermal performance. The thermal performance parameters for the cylindrical pin-fins, the large diameter cylindrical pin-fins, the diamond pin-fins and the triangular pin-fins are approximately 22.3%, 17.9%, 41.5%, and 47.0% lower than that of the optimized model, respectively.

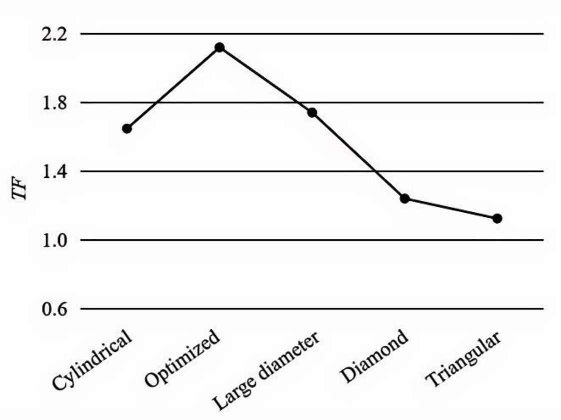

Fig. 12 Comparison of thermal performance parameters for the channels with different pin-fin designs

6. Conclusions

This paper employs the level set method in topology optimization to enhance the thermal performance of pin-fin cooling channels in gas turbine blades. Using pressure loss minimization as the objective function, comparing the optimized model with the baseline cylindrical pin-fin model and the channels with matched solid volume fraction of the optimized model, using the cylindrical pin-fin with larger diameter, the diamond pin-fin, and the triangular pin-fin, under a Reynolds number of 10,000. The conclusions drawn from this comparison are as follows:

1) The optimized channel disturbance elements exhibit complex shapes that vary in the streamwise, lateral, and pin-fin height directions, adapting to local flow and heat transfer conditions. A tadpole structure is observed downstream of the pin-fins, and the solid volume of the channel has increased compared to the baseline cylindrical pin-fin.

2) The area averaged Nu/Nu_0 of the optimized model is the highest. The area averaged Nu/Nu_0 for the baseline cylindrical pin-fin, the large diameter cylindrical pin-fin, the diamond pin-fin and the triangular pin-fin are approximately 32.7%, 4.7%, 12.5%, and 4.4% lower than that of the optimized model, respectively. After considering that the heat transfer areas are inconsistent among the five models studied, the optimized model still exhibits the highest Nu_T, with the Nu_T of the cylindrical pin-fins, the large diameter cylindrical pin-fins, the diamond pin-fins and the triangular pin-fins being approximately 28.8%, 7.4%, 9.5%, and 1.8% lower than that of the optimized model, respectively.

3) The optimized model has a lower pressure loss. The pressure loss of the cylindrical pin-fins is approximately 35.1% lower than that of the optimized model, while the pressure losses of the large diameter cylindrical pin-fins, the diamond pin-fins and the triangular pin-fins are approximately 53.9%, 232.7%, and 486.0% higher than that of the optimized model, respectively. The optimized model exhibits the highest thermal performance parameters, with the thermal performance parameters for the cylindrical pin-fins, the large diameter cylindrical pin-fins, the diamond pin-fins and the triangular pin-fins are approximately 22.3%, 17.9%, 41.5%, and 47.0% lower than that of the optimized model, respectively.

Acknowledgment

The authors gratefully acknowledge the financial supports for the project from National Nature Science Foundation of China (grant No.:52106047).

Nomenclature

A	-Area of the grid cell,[m^2]
A_0	-Area of the upper and lower walls and the surface of the pin-fins,[m^2]
C	-Constraint,[-]
D_h	-Hydraulic diameter,[mm]
f	-Friction coefficient $(=\frac{2D_h}{\rho U_{in}{}^2}\left\lvert\frac{\Delta p}{dx}\right\rvert)$,[-]
F	-Interfacial velocity,[m/s]
h	-Heat transfer coefficient $(=q/(T_w - T_c))$,[W/(m^2 ·K)]
k_f	-Thermal conductivity of the fluid,[W/m·K]
k	-Number of iterations,[-]
Nu	-Nusselt number $(=hD_h/k_f)$,[-]
p	-Fluid pressure,[Pa]
P_{in}	-Average pressure at the inlet surface boundary,[Pa]
P_{out}	-Average pressure at the outlet surface boundary,[Pa]
Pr	-Prandtl number,[-]
q	-Wall heat flux,[W/m^2]
Re	-Reynolds number$(=\rho U_{in}D_h/\mu)$,[-]
R	-Residual vector function,[-]
S	-Source term of the level set function,[-]
S_1	-Discrete vector field,[-]
T_w	-Wall temperature,[K]
T_c	-Bulk fluid temperature,[K]
TF	-Comprehensive heat transfer efficiency evaluation factor $(=\frac{Nu/Nu_0}{(f/f_0)^{1/3}})$,[-]
U_{in}	-Inlet velocity,[m/s]
V	-Volume of the grid cell,[m^3]
	Greek symbols
ρ	-Density,[kg/m3]
μ	-Dynamic viscosity,[Pa·s]
μ_t	-Turbulent viscosity,[Pa·s]
τ	-Pseudo-time,[-]
φ	-Level set variable,[-]
ω	-Constant source strength,[-]
λ	-Lagrange multiplier,[-]
β	-Penalty parameter,[-]
δ	-Thickness of the interface,[m]
α	-Brinkman penalty magnitude,[-]
Ω_{in}	-Design domain,[-]

References

[1] Zhang, L., *et al.*, Film cooling characteristic on trailing edge cutback of gas turbine airfoils with dimple/protrusion structure, *Journal of Chinese Society of Power Engineering, 40* (2020), 1, pp. 31-38+50

[2] Chyu, M. K., Siw, S. C., Recent advances of internal cooling techniques for gas turbine airfoils, *Journal of Thermal Science and Engineering Applications*, *5* (2013), 2, 021008

[3] Yeranee, K., Rao, Y., A review of recent studies on rotating internal cooling for gas turbine blades, *Chinese Journal of Aeronautics, 34* (2021), 7, pp. 85-113

[4] Metzger, D. E., *et al.*, Developing heat transfer in rectangular ducts with arrays of short pin fins, *American Society of Mechanical Engineers*, *1* (1982), 4, pp. 700-706

[5] Pandit, J., *et al.*, Effect of pin fin to channel height ratio and pin fin geometry on heat transfer performance for flow in rectangular channels, *International Journal of Heat and Mass Transfer, 77* (2014), pp. 359–368

[6] Yalçınkaya, O., *et al.*, Thermal performance of elliptical pins on a semicircular concave surface in the staggered array jet impingement cooling, *Applied Thermal Engineering, 231* (2023), 120998

[7] Yalçınkaya, O., *et al.*, Assessment of convective heat transfer characteristics for elliptical-shaped pin-roughened surface for the jet impingement cooling, *ASME Journal of Heat and Mass Transfer, 145* (2023), 2, 022301

[8] Chyu, M. K., *et al.*, Comparison of heat transfer from staggered pin fin arrays with circular, cubic and diamond shaped elements, *ASME Turbo Expo*, (2007), pp.991–999

[9] Zhang, H., Ke, Y., Overview of the present situation and application of additive manufacturing, *Packaging Engineering, 42* (2021), 16, pp. 9-15

[10] Li, Z., *et al.*, Research review of advanced light alloy materials and forming technology in aerospace, *Shanghai Aerospace, 36* (2019), 2, pp. 9-21

[11] Hen, Y., *et al.*, Research and application of additive manufacturing technology in the field of spacecraft, *Xi'an: International Fo-rum on High-end Equipment Engineering Management Facing Additive Manufacturing and New Generation Information Technology*, (2020)

[12] Li, D., *et al.*, Additive manufacturing-revolutionary technology for leading the aerospace manufacturing, *Acta Aeronautica et Astronautica Sinic*a, *43* (2022), 4, 525387

[13] Zhang, P., Topology optimization of blended lattices microstructure for additive manufacturing, Master thesic, Henan Polytechnic University, Jiaozuo, China, 2023

[14] Alexandersen, J., Andreasen, C. S., A review of topology optimisation for fluid-based problems, *International Journal for Numerical Methods in Fluids, 5* (2020), 1, 29

[15] An, L., Topology optimization of fluid-solid conjugate heat transfer structure, Master thesis, Dalian University of Technology, Dalian, China, 2020

[16] Borrvall, T., Petersson, J., Topology optimization of fluids in Stokes flow, *International Journal for Numerical Methods in Fluids, 41* (2003), 1, pp. 77-107

[17] Yoon, G. H., Topology optimization for turbulent flow with Spalart-Allmaras model, *Computer Methods in Applied Mechanics and Engineering, 303 (*2016), pp. 288-311

[18] Yoon, G. H., Topology optimization method with finite elements based on the k-ε turbulence model, *Computer Methods in Applied Mechanics and Engineering, 361* (2020), pp. 15-18

[19] Yeranee, K., *et al.*, Enhanced thermal performance of a pin-fin cooling channel for gas turbine blade by density-based topology optimization, *International journal of thermal sciences, 181* (2022), 107783

[20] Yeranee, K., Rao, Y., Turbulent flow and heat transfer enhancement for turbine blade trailing edge cooling with gyroid-type triply periodic minimal surfaces, *Journal of Engineering for Gas Turbines and Power*, *145* (2003), 7, 071008

[21] Wang, Z., *et al.*, Performance comparison of battery cold plates designed using topology optimization across laminar and turbulent flow regime, *International Journal of Heat and Mass Transfer*, *238* (2025), 126450

[22] Pandey, V., Lee, P. S., Fluid dynamic investigation of a topology-optimized liquid-cooled heat sink for enhanced performance, *Physics of Fluids, 37* (2025), 3

[23] Duan, X. B., *et al.*, Shape-topology optimization for Navier-Stokes problem using variational level set method, *Journal of Computational and Applied Mathematic*s, *222* (2008), pp. 487–499

[24] Jiang, Z., A study on fluid channel topology optimization method based on parameterized level set method, Master thesic, South China University of Technology, Guangzhou, China, 2021

[25] Haertel, J. H. K., *et al.,* Topology optimization of a pseudo 3D thermofluid heat sink model, *International journal of heat and mass transfer, 121* (2018), pp. 1073-1088.

[26] Ye, Y., *et al.,* Heat transfer characteristics of a cooling structure with a combination of inclined impact and column ribs, *Journal of Engineering Thermophysics, 40* (2019), 2, pp. 389-395

[27] Rao, Y., *et al.,* An experimental study of pressure loss and heat transfer in the pin fin-dimple channels with various dimple depths, *International journal of heat and mass transfer, 55* (2012), pp. 6723-6733

[28] Ligrani, P., Heat transfer augmentation technologies for internal cooling of turbine components of gas turbine engines, *International journal of rotating machinery*, *1* (2013), 275653

Received: 07.04.2025.

Revised: 20.05.2025.

Accepted: 07.06.2025.